OPEN ACCESS
Journal of Innovative Optical Health Sciences
Vol. 15, No. 5 (2022) 2250034 (12 pages)

DOI: 10.1142/S1793545822500341

World Scientific
www.worldscientific.com

Fluorescence emission difference microscopy based on polarization modulation

Wanjie Dong*, Yuran Huang*, Zhimin Zhang†,‖, Liang Xu*, Cuifang Kuang*,†,‡,§,**, Xiang Hao*, Liangcai Cao¶ and Xu Liu*

*State Key Laboratory of Modern Optical Instrumentation
College of Optical Science and Engineering
Zhejiang University, Hangzhou 310027, P. R. China

†Research Center for Intelligent Chips and Devices
Zhejiang Lab, Hangzhou 311121, P. R. China

‡Ningbo Research Institute, Zhejiang University
Ningbo, Zhejiang 315100, P. R. China

§Collaborative Innovation Center of Extreme Optics
Shanxi University, Taiyuan 030006, P. R. China

¶State Key Laboratory of Precision Measurement
Technology and Instruments, Department of Precision Instruments
Tsinghua University, Beijing 100084, P. R. China

‖z_zhimin@zhejianglab.com

**cfkuang@zju.edu.cn

Received 2 June 2022
Accepted 28 July 2022
Published 28 September 2022

In this paper, we propose a new fluorescence emission difference microscopy (FED) technique based on polarization modulation. An electro-optical modulator (EOM) is used to switch the excitation beam between the horizontal and vertical polarization states at a high frequency, which leads to solid- and donut-shaped beams after spatial light modulation. Experiment on the fluorescent nanoparticles demonstrates that the proposed method can achieve $\sim \lambda/4$ spatial resolution. Using the proposed system, the dynamic imaging of subcellular structures in living cells over time is achieved.

Keywords: Super-resolution; fluorescence emission difference microscopy; electro-optical modulator; polarization modulation.

1. Introduction

Confocal fluorescence microscopy has been a powerful tool in many research fields because of its ability to obtain noninvasive serial optical sections of living cells as well as a marginal improvement in lateral resolution compared to wide-field microscopy.[1] However, the resolution of confocal fluorescence microscopy is limited to approximately half the wavelength by the diffraction limit. To achieve higher spatial resolution, several super-resolution fluorescence microscopy methods, such as photo-activated localization microscopy (PALM),[2] stochastic optical reconstruction microscopy (STORM),[3] stimulated emission depletion microscopy (STED),[4] and structured illumination microscopy (SIM),[5] have been proposed over the past few decades. In addition to the above methods, fluorescence emission difference microscopy (FED) achieves super-resolution by subtracting two images acquired under different point-scanning excitation beams (solid- and donut-shaped).[6] The method of FED to achieve super-resolution is similar to STED to a certain extent, since STED uses a solid-shaped beam to excite fluorescence and a donut-shaped beam to deplete the margin area of the fluorescence spot to reduce the size of the fluorescence spot. Due to the advantages of lower light intensity requirements, simpler optical setup and a wider range of available dyes, FED is easier to implement and has a wide range of applications in the field of practical scientific research. Recent progress in FED microscopy development, such as combining the saturated fluorescence emission effect,[7] higher-order vector beams,[8] and two-photon microscopy[9] have been reported to improve spatial resolution. FED microscopy has a great potential in biomedical imaging because of its minimal requirements for sample preparation, low illumination intensities, and simple processing procedures.

In earlier FED methods, two images, confocal and negative confocal images, were captured under two scanning processes before subtracting the operation, thereby limiting its temporal resolution. The mechanical instability of the system and environmental noise between the two scanning processes can affect the resolution, authenticity, and signal-to-noise ratio (SNR) of the system.[10] In particular, when imaging moving or living biological samples, artifacts may occur, which restrict the application of FED microscopy in the investigation of live cell dynamics and real-time imaging. In previous studies, Cai *et al.* proposed a single-exposure FED microscopy that utilizes high-speed vector polarization modulation to achieve rapid conversion of cylindrical vector optical field between radially and azimuthally polarization states.[11] In the experiments, by adjusting the optical frequencies of two circularly polarized beams with opposite handedness, they could be synthesized to obtain a beam that switches between radially and azimuthally polarization states after passing through a first-order vortex phase plate.[11] However, two excitation light paths were required, which could lead to an increase in the complexity of the experimental system and errors.

In this paper, we propose a FED microscopy using an electro-optical modulator (EOM) and a spatial light modulator (SLM) to achieve high-speed switching between solid- and donut-shaped excitation beams during the scanning process. This method avoids the secondary scanning process and achieves real-time imaging without post processing. The EOM can achieve fast switching of the light polarization direction between the horizontal and vertical states, and the polarization-sensitive SLM only modulates the light when its polarization direction is parallel to the modulation direction of the SLM. Therefore, a rapid transition of light between the two states can be achieved after being modulated by the EOM and SLM. The fast conversion between horizontally and vertically polarized beams allows differential fluorescence signals to be obtained during the scanning process and effectively reduces the time difference between the solid- and donut-shaped signals. By imaging the morphology and dynamics of subcellular structures, the proposed FED microscopy method could effectively eliminate mechanical instability and artifacts and could be widely used in live cell imaging.

2. System and Methods

2.1. *Polarization modulation-based fluorescence emission difference microscopy system*

The schematic of the experimental setup is shown in Fig. 1. The system incorporates a polarization modulation module in a conventional FED system. The light source is a picosecond diode laser with a

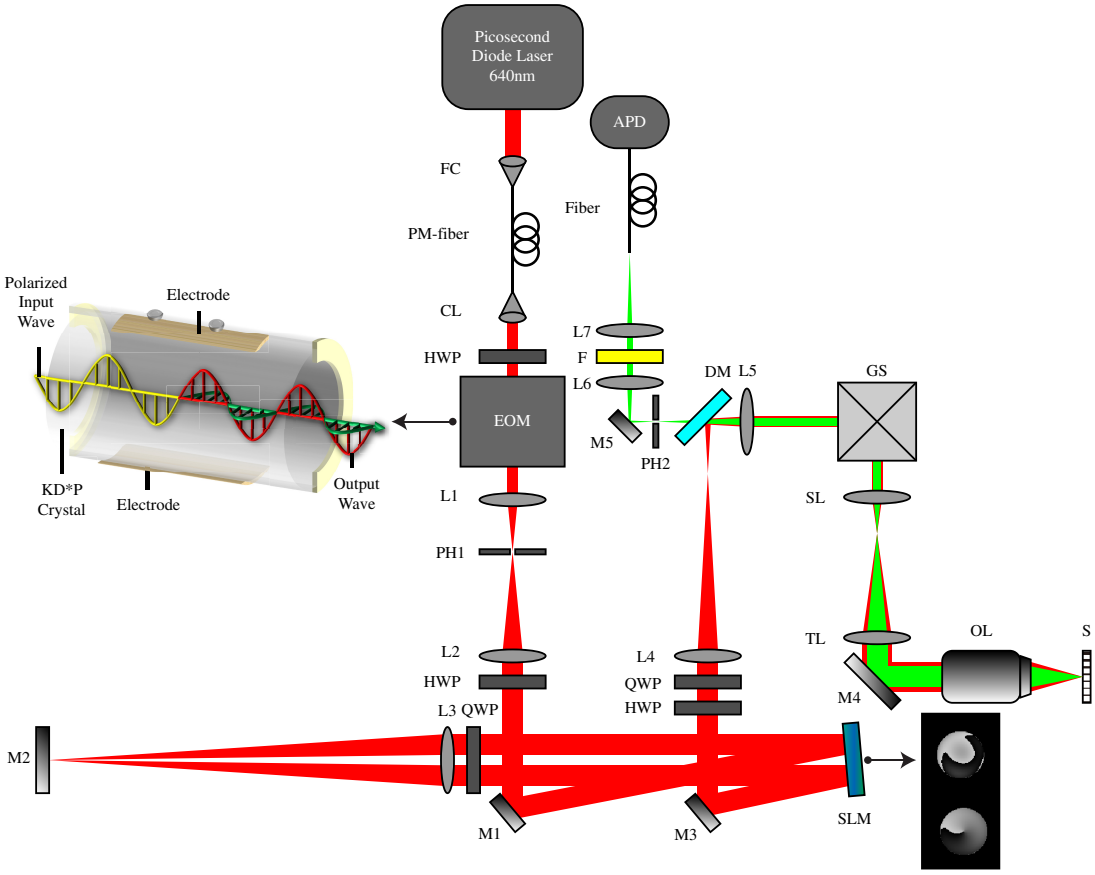

Fig. 1. Schematic diagram of the proposed FED based on fast-speed polarization modulation. PM-fiber: Polarization-maintaining fiber; FC: Fiber coupler; CL: Collimator; HWP: Half-wave plate; EOM: Electro-optical modulator; L: Lens; PH: Pinhole; M: Mirror; SLM: spatial light modulator; QWP: quarter-wave plate; DM: dichroic mirror; GS: Galvanometer scanner; SL: Scanning lens; TL: Tube lens; OL: 100× objective lens in oil; S: Sample; F: Filter; APD: Avalanche photodiode.

center wavelength of 640 nm at 80 MHz repetition rate. The light is first coupled into a single-mode polarization-maintaining fiber through a coupler and then expanded and collimated by the collimator to match the aperture of the EOM. Then, the light passes through a half-wave plate (HWP) and becomes a linearly polarized light of specific angle to meet the polarization requirements of the EOM. An EOM (Conoptics, Model 350-80 KD*P Series E-O Modulator) is used to achieve fast switching of light between the horizontally and vertically polarized states. The driving frequency of the amplifier that drives the EOM can reach 8 MHz and is synchronized with the drive signal of the galvanometer. In the experiment, the driving frequency is influenced by the single point exposure time of the sample and can be modulated by a software. After passing through the EOM, a beam expander system consisting of two lenses (L1 and L2 in Fig. 1) is used to expand the beam and a HWP is used to adjust the polarization direction of the light. Since the phase modulation of the SLM (Hamamatsu, LCOS-SLM Serial No.:LSH0802678) can only act on one linear polarization, when the light is horizontally polarized after EOM modulation, it is only modified on the first pass of the SLM and vertically polarized after double passing through a quarter-wave plate (QWP). The SLM is re-imaged onto itself through the lens (L3 in Fig. 1) after being reflected by the mirror (M2 in Fig. 1) located at the focal plane position of the lens, and the light is not modified during the second pass of the SLM. When the light is vertically polarized after EOM modulation, it is modified only on the second pass of the SLM after double passing through the QWP. The different positions of the SLM are loaded with different patterns, so that the light can be modulated to different states (solid- and donut-shaped beams) and the aberrations of the system can be compensated by adding Zernike phase functions to the

modulation parameters of the SLM[12,13] when it is switched between different polarization states. Then the light is subjected to polarization rotation by a HWP and a QWP to ensure perfect circular polarization so that the central intensity of the donut-shaped beam is minimized. A 4f system consisting of two lenses (L4 and L5 in Fig. 1) is used to adjust the beam size and relay the excitation light. A dichroic mirror (DM) is placed before the galvanometer scanner (GS) to separate the excitation light and fluorescent light. The GS controlled by a National Instruments card is used to realize two-dimensional fast scan of the sample. The excitation light is then relayed by a scanning lens (SL) and a tube lens (TL) after the GS and is focused on the sample plane using an objective lens (Nikon, 100× oil immersion) with NA of 1.49.

The fluorescent light is collected by the same objective lens, relayed by the TL and SL, descanned by the GS, and separated from the excitation light through the dichroic mirror. Then, the fluorescent light is delayed and adjusted by a 4f system consisting of two lenses (L5 and L6 in Fig. 1), spectrally filtered by a bandpass filter, focused by a lens (L7 in Fig. 1) onto a multimode optical fiber, and transmitted into an avalanche photodiode (APD, Excelitas Technologies, SPCM-AORH-10-FC). A pinhole is used to remove noise and further improve the imaging quality of the system. The APD is driven by a signal synchronized with the drive signals of the GS and the EOM. The differential fluorescence signal is extracted when the fast switching of excitation light between different states is completed and is displayed in real time during the scanning process. The integral setup is controlled by two National Instruments cards (National Instruments, NI card 6363 and NI card 4461).

2.2. *Polarization modulation*

The EOM is made of electro-optic crystals, such as lithium niobate ($LiNbO_3$), gallium arsenide (GaAs), and potassium dihydrogen phosphate (KDP) crystals.[14–17] In this experimental system, an EOM made of KDP crystal is used to realize the fast switching of the light polarization direction between the horizontal and vertical states. According to the electro-optical effect, under the action of an external electric field, the refractive index $n(E)$ of the electric optical material is a function of the amplitude of the external electric field, which can be written as follows:

$$n(E) \approx n - \frac{1}{2}\gamma n^3, \tag{1}$$

where γ is the Pockels coefficient of the electric optical material. The Pockels effect observed in certain crystals and electro-optic polymers[18,19] gives rise to a linear change in the refractive index with an applied electric field.[20] Any polarized light can be decomposed into two orthogonal polarization components. In an anisotropic medium, these two components are generally decomposed into two main refractive index axes of a refractive index ellipsoid. We label the refractive indices corresponding to the two polarization components as n_1 and n_2. Because of the difference in the propagation speeds of the two components, when one component propagates to the other end of the device, it will lead or lag behind the other component, thereby forming a phase delay and changing the polarization state of the emitted light. When an external electric field E is applied to an anisotropic material and light passes through an EOM of length L, according to the Pockels effect, the phase difference between the two polarization components can be written as follows:

$$\begin{aligned}\Gamma &= k_0[n_1(E) - n_2(E)]L \\ &= k_0(n_1 - n_2)L - \frac{1}{2}k_0(\gamma_1 n_1^3 - \gamma_2 n_2^3)EL,\end{aligned} \tag{2}$$

where γ_1 and γ_2 are Pockels coefficients along the directions of the two polarization components. For a transverse modulator with the direction of the applied electric field perpendicular to the direction of light propagation, the electric field is expressed as follows:

$$E = V/d, \tag{3}$$

where V is the applied voltage and d is the distance between the two electrodes. The expression for the phase difference can be written as follows:

$$\begin{aligned}\Gamma &= k_0(n_1 - n_2)L - \pi\frac{VL}{d\lambda_0}(\gamma_1 n_1^3 - \gamma_2 n_2^3) \\ &= \Gamma_0 - \pi\frac{V}{V_\pi},\end{aligned} \tag{4}$$

where $\Gamma_0 = k_0(n_1 - n_2)L$ is the phase difference of the device itself, and the half-wave voltage V_π can

be written as follows:

$$V_\pi = \frac{d}{L}\frac{\lambda_0}{\gamma_1 n_1^3 - \gamma_2 n_2^3}. \tag{5}$$

When the applied voltage is V_π, the phase difference is π.

Linearly polarized light with an angle of 45° between its polarization direction and the crystal optical axis of the EOM can be decomposed into two components with the same intensity, one of which is polarized parallel to the crystal optical axis and the other is polarized perpendicular to the crystal optical axis. Adjusting the magnitude of the bias voltage of the EOM when the phase difference between the two polarization components is zero, the polarization direction of the emergent light is the same as that of the incident light. By adjusting the driving voltage of the EOM, the phase difference between the two polarization components can be changed to π, and the polarization direction of the emergent light is perpendicular to the polarization direction of the incident light. By adjusting the driving voltage of the EOM, the polarization direction of the light can be changed after being modulated by the EOM. Due to its high modulation speed, EOM can achieve the fast switching of light polarization direction.

2.3. *Fluorescence emission difference microscopy*

In FED, a conventional confocal image acquired when the sample is excited with a solid-shaped beam and a negative confocal image acquired when the sample is excited with a donut-shaped beam must be obtained.[6] The super-resolution FED image is obtained by subtracting the negative confocal image from the conventional confocal image as follows:

$$I_{\mathrm{FED}} = I_c - \gamma \cdot I_n, \tag{6}$$

where I_{FED} is the FED image, I_c is the normalized intensity distribution of the confocal image, I_n is the normalized intensity distribution of the negative confocal image, and γ is the subtractive factor. In the processing of subtraction, negative values of intensity which is physically unrealistic will be produced. So, the removal of negative values is required to get the final intensity distribution of the FED image I_f and can be expressed as follows:

$$I_f = \begin{cases} I_{\mathrm{FED}} & I_{\mathrm{FED}} \geq 0 \\ 0 & I_{\mathrm{FED}} < 0 \end{cases}. \tag{7}$$

The subtractive factor γ plays a critical role in improving the performance of imaging resolution and should be related to the parameters of the excitation beams and the properties of the samples.[21] In the conventional FED methods, the transition between the two states (solid- and donut-shaped) of the beam is usually performed after scanning a complete image due to the time it takes to transition between the two states. Since the EOM can respond to a driving signal with a rising or falling edge of 50 ns and a frequency of 8 MHz, the time required to convert the polarization direction of the excitation light between horizontally and vertically polarized is much lower than the microsecond single-point exposure time commonly used in experiments. So, it is possible to switch the state of the excitation light after each line of scanning is completed without affecting the imaging results. Switching the spot state with EOM modulation and scanning again after each line of scanning is completed, no additional switching time is introduced, and the time difference between the corresponding points in the confocal and negative confocal images is reduced from the time required for scanning a complete image to the time required for scanning a line in the image. As for image consisting of 500×500 pixels, the time difference between the corresponding pixels in confocal and negative confocal images is reduced by a factor of 500 compared to the traditional FED method.

Different combinations of beam shapes can be used to achieve FED microscopy, such as the circular polarized Gaussian beam and vortex-phase-plate-generated donut beam,[6,22] or the vector radially polarized solid beam and azimuthally polarized donut beam.[23] In this paper, the former combination is used to achieve FED microscopy. After being modulated by the EOM, when the polarization direction of the light is parallel to the modulation direction of the polarization-sensitive SLM, the SLM modulates the light with a $0 - 2\pi$ vortex phase modulation pattern and the beam will be donut-shaped. When the polarization direction is perpendicular to the modulation direction of the SLM, the beam will be solid-shaped. The differential imaging performance of the method used in this paper is

calculated theoretically and the corresponding results are shown in Fig. 2. As shown in Figs. 2(a) and 2(b), the horizontally polarized beam produces a donut-shaped spot and the vertically polarized beam produces a solid-shaped spot. Figure 2(c) shows the differential image produced by subtracting the images scanned by the horizontally and vertically polarized beams. Figure 2(d) illustrates that the full width at half maximum (FWHM) of the differential intensity can reach below ∼0.5, compared to the FWHM of the confocal intensity.

2.4. *Aberration correction*

In addition to phase modulating the light to obtain the desired intensity distribution, the SLM can also be used to correct for optical aberrations in the system or the sample.[24] Aberrations present in the system can be compensated by addition of phase functions described by Zernike polynomials.[12] To maximize the image quality of the system, each part of the SLM is fully utilized to compensate for both solid and hollow spot aberrations. In addition to compensating for multiple aberrations described by Zernike Polynomials, including defocus, astigmatism, coma and spherical aberration, the SLM is also used to adjust the position and tilt of the beam to ensure that the solid and hollow spots coincide on the imaging plane. In order to simplify the complexity of aberration compensation, only the above-mentioned aberrations having major impact on image quality are compensated. To increase the

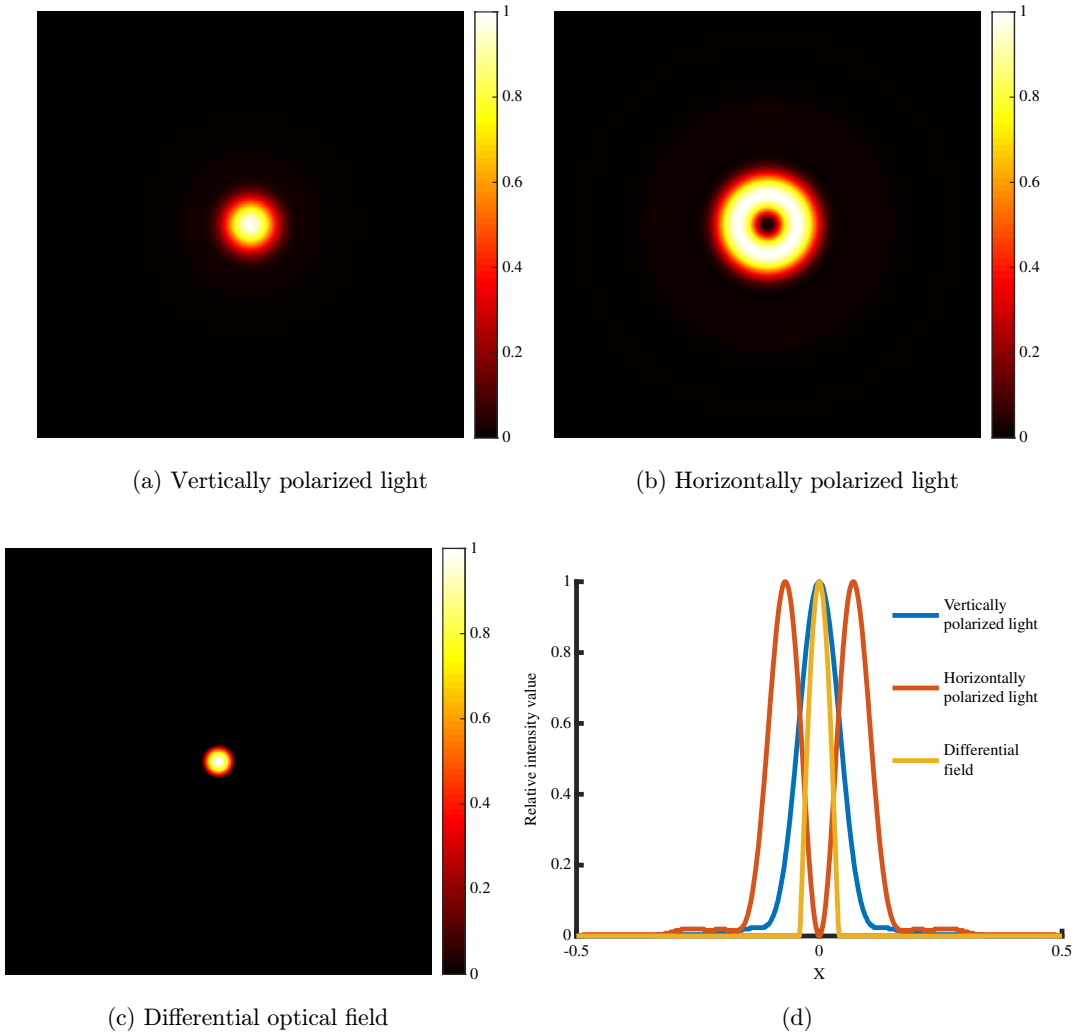

(a) Vertically polarized light

(b) Horizontally polarized light

(c) Differential optical field

(d)

Fig. 2. Theoretical calculations of FED imaging. (a) Total field intensity distribution of vertically polarized light; (b) total field intensity distribution of horizontally polarized light; (c) differential distribution between vertically polarized light and horizontally polarized light; (d) cross-sections of beam profiles for (a) vertically polarized light (blue curve), (b) horizontally polarized light (red curve), and (c) differential field (yellow curve).

imaging speed while minimizing photobleaching of the sample, system aberrations are compensated for before the experiment rather than during the experiment. The aberration compensation process is achieved by imaging the standard gold nanoparticles with the experimental system and adjusting the amplitudes of the appropriate phase functions to obtain the desired light intensity distribution.

3. Results and Discussion

3.1. *Results of nanoparticles*

We imaged 40 nm fluorescent nanoparticles (Abberior, red flour. 40 nm) to verify the resolution enhancement of our FED system. The experimental results and resolution calculation results of the fluorescent beads are shown in Fig. 3. Figures 3(a) and 3(b) present the results of confocal and FED imaging. The cross-sections of fluorescence intensity along the white lines labeled in Figs. 3(a) and 3(b), which are fitted using a Gaussian profile, and enlargement of white-boxed regions in Figs. 3(a) and 3(b) are shown in Figs. 3(c) and 3(d). The cross-sections of the fluorescence intensity along the yellow lines labeled in Figs. 3(a) and 3(b) are fitted using a Gaussian profile and the enlargement of yellow-boxed regions in Figs. 3(a) and 3(b) are shown in Figs. 3(e) and 3(f). The FWHM of the FED image is 160 nm, which is nearly one-quarter of the wavelength of the excitation light. The two fluorescent beads that are indistinguishable in the confocal image can be clearly distinguished in the FED image. Because the time difference between the two scans is effectively reduced, the noise caused by mechanical instability can be effectively avoided. Decorrelation analysis is used to calculate the resolution of our FED system.[25] The decorrelation analysis requires only a nonsaturated and bandwidth-limited signal with adequate spatial sampling, and is based on partial phase correlation while it does not rely on user-defined parameters,[25] so it can be used to estimate the resolution of our system. Decorrelation analysis of the confocal image in Fig. 3(a) is shown in Fig. 3(g) and the decorrelation analysis of the FED image in Fig. 3(b) is shown in Fig. 3(h). The resolution can be calculated as follows:

$$\text{Resolution} = \frac{2 \times \text{pixel size}}{k_c}, \tag{8}$$

where k_c is the spatial frequency expressed in normalized frequencies.[25] The resolution of confocal imaging is 358.43 nm and the SNR of confocal imaging is 0.342 calculated by decorrelation analysis, meanwhile, the resolution of FED imaging is 159.8 nm and the SNR of FED imaging is 0.57.

3.2. *Results of mitochondria*

To verify the feasibility of our system for live-cell imaging, mitochondria stained with fluorescent probes in live U2OS cells were imaged. U2OS cells were obtained and cultured in an incubator at 37°C and 5% CO_2. U2OS cells were cultivated in McCoy's 5A medium (Gibco) supplemented with 10% FBS (Gibco). Cells were seeded in 35 mm glass-bottom dishes (Thermo Fisher Scientific, Inc.). After overnight incubation, the cells were washed thrice with phosphate-buffered saline. For labeling mitochondria in live U2OS cells, MitoTracker Deep Red FM (Yeasen, Inc.) was dissolved in 10 μL dimethyl sulfoxide (DMSO), and then diluted with phosphate-buffered saline to 200 μL (750 nM). The cells were incubated with the probe solution in a 5% CO_2 atmosphere at 37°C for 30 min. Afterwards, the supernatant was discarded, and the cells were stained with 10 mg/ml trypan blue and then washed gently thrice with phosphate-buffered saline. For imaging, the supernatant was changed in advance to phenol red-free DMEM (Thermo Fisher Scientific).

As shown in Fig. 4, mitochondria appear as long, tubular, or branched structures and are responsible for generating metabolic energy for cells; they also participate in the aging, disease, and developmental processes of cells.[26] The imaging results of the conventional confocal imaging system and proposed FED system are shown in Figs. 4(a) and 4(b). The bending and extension of the mitochondria in a live U2OS cell were captured by our FED system, as shown in Figs. 4(c) and 4(d). The cross-sections of the fluorescence intensity along the white lines are labeled in Figs. 4(a) and 4(b), which are fitted using a Gaussian profile, and the enlargement of yellow-boxed regions in Figs. 4(a) and 4(b) are shown in Figs. 4(e) and 4(f), illustrating that compared with conventional confocal microscopy, the imaging results of the FED system can more clearly display and distinguish structures on the mitochondrial surface. Raw data (500 × 500 pixels) were acquired with a single point exposure time of 6 μs and pixel

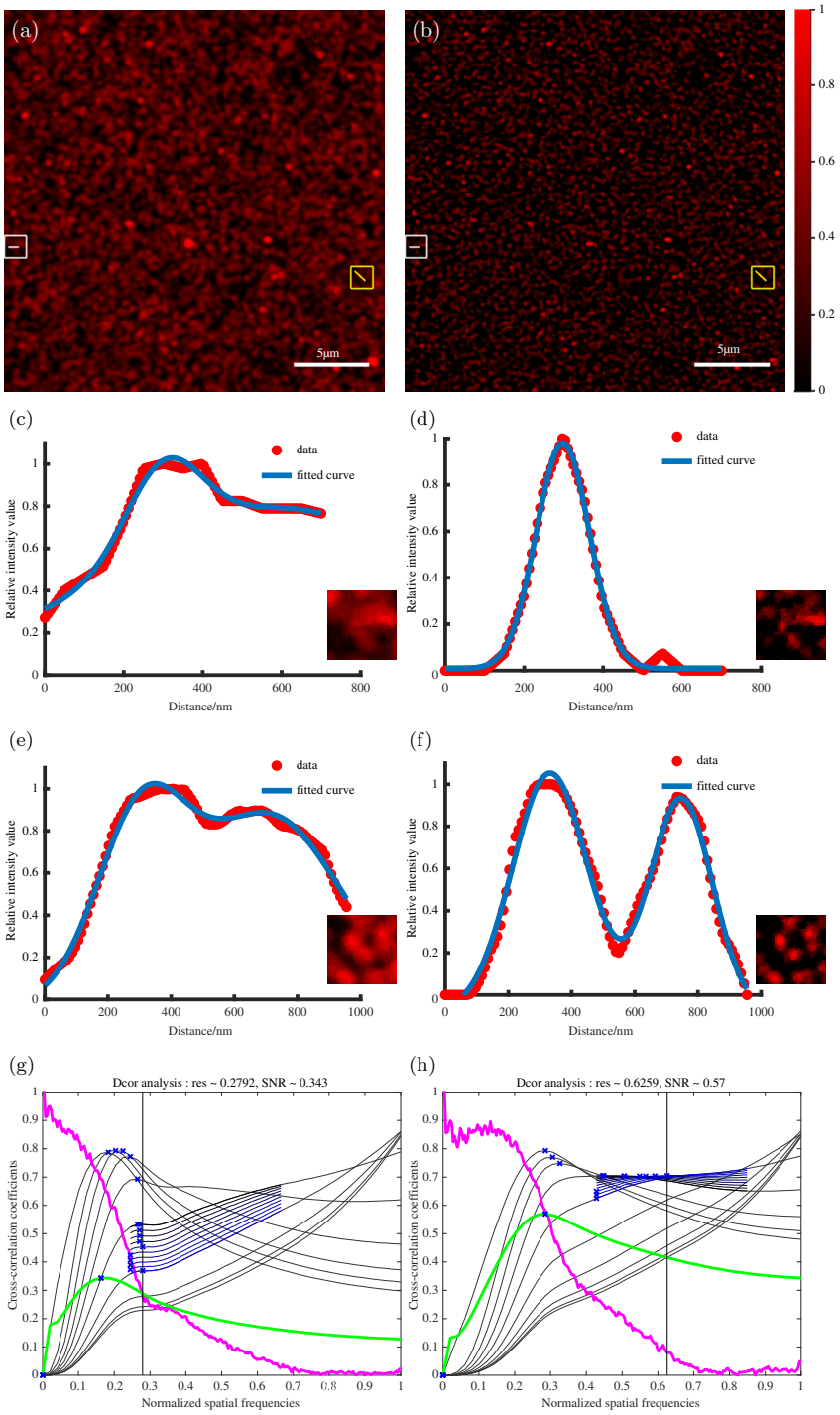

Fig. 3. Imaging results and resolution calculation results of 40 nm fluorescent nanoparticles imaging by proposed FED microscopy and conventional confocal microscopy system. (a) Confocal image; (b) FED image; (c), (d) enlargement of white-boxed regions in (a), (b), and normalized intensity profiles along the white lines labeled in (a), (b); (e), (f) enlargement of yellow-boxed regions in (a), (b) and normalized intensity profiles along the yellow lines labeled in (a), (b); (g), (h) corresponding decorrelation analyses of (a) and (b). Green lines in (g) and (h) represent decorrelation functions before high-pass filtering, magenta lines represent radial average of log of absolute value of Fourier transform of (a) and (b), gray lines represent decorrelation functions with high-pass filtering, blue and black lines represent decorrelation functions with refined mask radius and high-pass filtering range, blue crosses represent local maxima of the decorrelation functions and dashed vertical lines represent cut-off spatial frequencies k_c. All data in (c), (d), (e) and (f) are fitted using a Gaussian function, the scale bar in (a) and (b) is 5 μm, pixel size is 50 nm, single point exposure time is 6 μs and subtraction factor is 0.7.

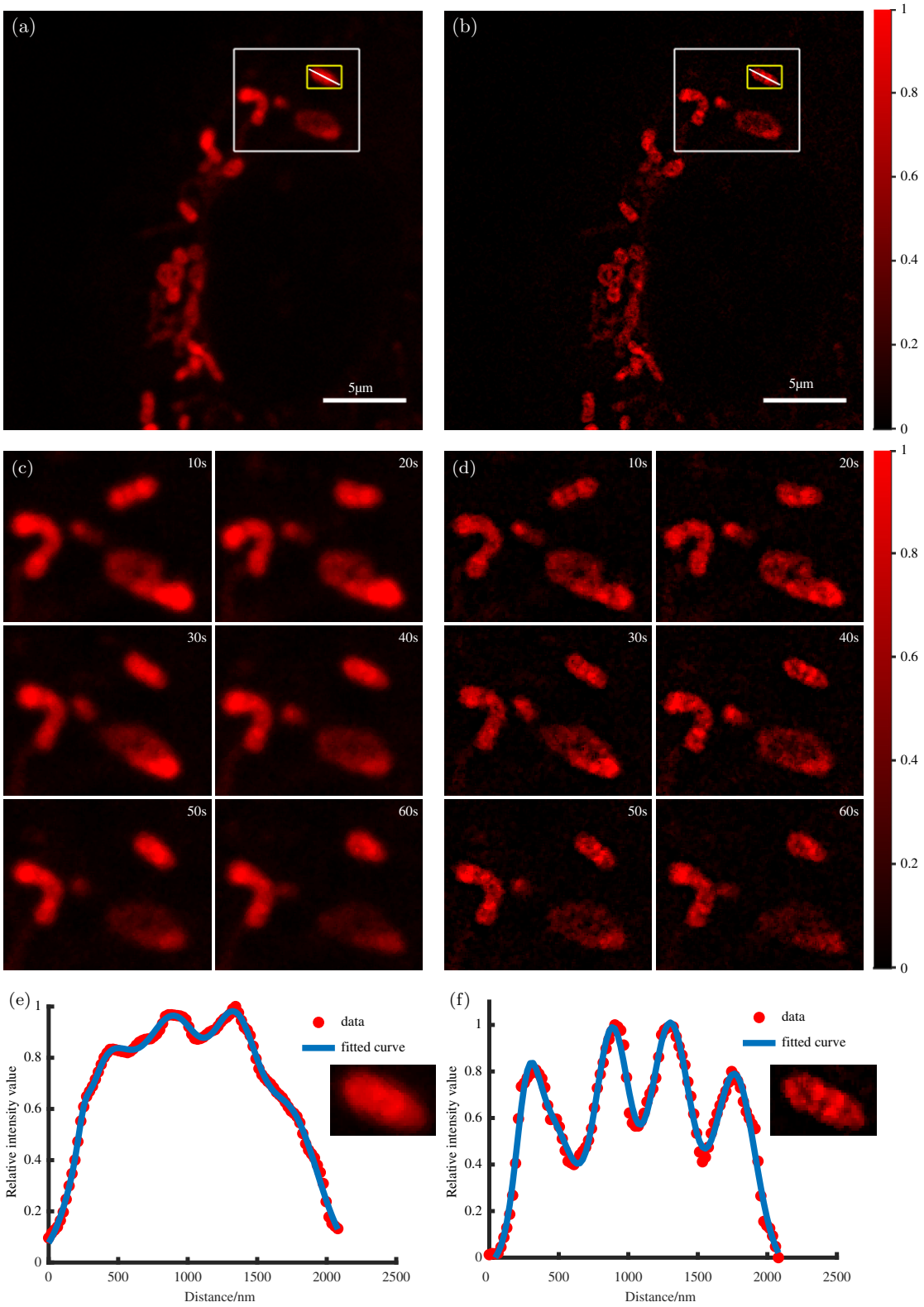

Fig. 4. Imaging results of mitochondria stained with fluorescent probes in live U2OS cells imaging by proposed FED microscopy system. (a) confocal image, (b) FED image, (c) and (d) magnified inset of white-boxed regions in (a) and (b), showing mitochondria structural dynamics; (e) and (f) enlargement of yellow-boxed regions in (a) and (b), and normalized intensity profiles along the white lines labeled in (a) and (b). All data are fitted using a Gaussian function, the scale bar in (a) and (b) is 5 μm, pixel size is 50 nm, single point exposure time is 6 μs and subtraction factor is 0.7.

size of 50 nm, indicating a field of view (FOV) of $25 \times 25\,\mu m^2$. Each frame requires 3.63 s recording time and the time difference between the corresponding pixels in confocal and negative confocal images is 3.63 ms, with the speed determined by the fluorophores and GS.

To verify the artifact-removing ability of our system, the imaging results of our FED system for mitochondria in live U2OS cells are compared with the conventional FED system. Pseudo-color maps composed of a superposition of confocal and negative confocal images obtained by the conventional FED system and our FED system are shown in Fig. 5, where the confocal image occupies the red channel and the negative confocal image occupies the green channel. Raw data (500×500 pixels) were acquired with a single point exposure time of $6\,\mu s$ and pixel size of 50 nm, indicating a FOV of $25 \times 25\,\mu m^2$. Each frame requires 3.63 s recording time, the time difference between the corresponding pixels in confocal and negative confocal images of the conventional FED system is 1.815 s, while the time difference of our FED system is 3.63 ms. From the result comparison, it can be clearly observed that in the result of the conventional FED system, the misalignment of mitochondria in the confocal and negative confocal images caused by the movement of the sample can be found, while in our FED system, this phenomenon is reduced.

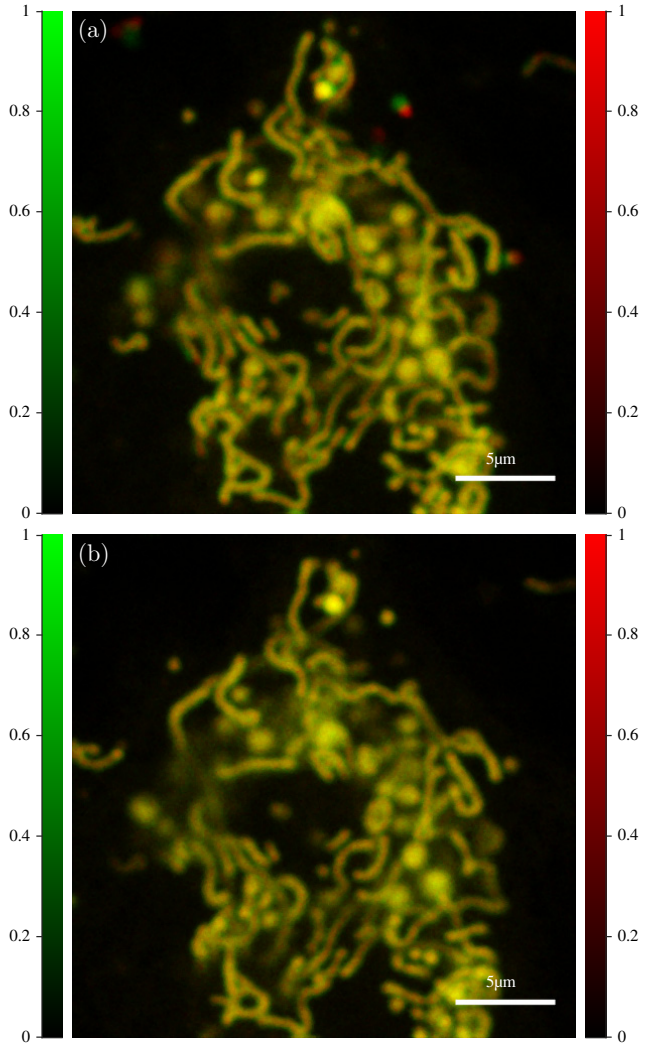

Fig. 5. Pseudo-color maps composed of confocal and negative confocal imaging results of mitochondria stained with fluorescent probes in live U2OS cells imaging by conventional FED microscopy system and proposed FED microscopy system. (a) conventional FED image; (b) proposed FED image. The scale bar in (a) and (b) is $5\,\mu m$, pixel size is 50 nm, and single point exposure time is $6\,\mu s$.

3.3. *Discussion*

FED microscopy is easy to implement and combine with other techniques to improve its imaging quality, which makes it have a wide range of applications. Since conventional FED methods needs to obtain confocal and negative confocal images to complete the subtraction operation, which usually requires two scanning processes, thereby limiting its temporal resolution. Besides, the time difference between the acquisition of the confocal and negative confocal images may also cause problems such as noise and artifacts that affect the imaging quality and restrict its application in the investigation of live cell dynamics and real-time imaging. In this paper, we proposed an FED microscopy method by adding an EOM to the FED system.

EOM can realize fast conversion of light between two polarization states of horizontal polarization and vertical polarization. Combined with a polarization-sensitive SLM, the conversion of the beam between solid- and donut-shaped states can finally be realized. By adjusting the optical path and loading different phase modulation parameters at different positions of the SLM, when the light is horizontally polarized, it will be modulated to obtain a donut-shaped spot, and when the light is vertically polarized, it will be modulated to obtain a solid-shaped spot. Compared with adjusting the modulation parameters of the SLM surface, only the driving voltage of the EOM needs to be adjusted to realize the conversion of the beam between different states, which greatly reduces the complexity of programming control. Since the EOM has a fast

response speed, the beam state can be converted during the scanning process without affecting the imaging effect.

Our proposed FED system can realize the conversion of the beam state after each line of scanning, effectively reducing the time difference between the same pixels of the solid- and donut-shaped beams, thereby improving the imaging quality, especially when imaging live cell samples, it can effectively eliminate artifacts. Our experiments show that mitochondria stained with fluorescent probes in live U2OS cells can be clearly imaged and the structures on the mitochondrial surface can be distinguished, demonstrating the resolution enhancement and ability to image living biological samples.

4. Conclusion

In conclusion, we proposed a FED microscopy method based on polarization modulation. The use of EOMs to adjust the excitation light to rapidly switch between two polarization states and SLMs to phase-modulate the excitation light, combined with the principle of fluorescence difference microscopy, leads to a new scheme for high-speed FED imaging. The new FED imaging method effectively eliminates artifacts by reducing the time interval between the conventional and negative confocal images on the same pixel from 1.815 s to 3.63 ms (when the image consisting of 500×500 pixels is acquired with a single-point exposure time of 6 μs) while reducing mechanical and environmental noise. In addition, our method reduces mechanical alignment errors using the same beam for modulation and imaging, which also enables artifact reduction. The experiments demonstrate that the proposed method can be widely used for the real-time imaging of living biological samples. To further improve the resolution and SNR of the proposed FED microscopy method, it can be combined with other super-resolution microscopic imaging techniques.

Conflicts of Interest

The authors declare that there are no conflicts of interest relevant to this paper.

Acknowledgments

This work was supported in part by the National Natural Science Foundation of China (61827825, 62125504, and 61735017), Major Program of the Natural Science Foundation of Zhejiang Province (LD21F050002), Key Research and Development Program of Zhejiang Province (2020C01116), Zhejiang Lab (2020MC0AE01), Zhejiang Provincial Ten Thousand Plan for Young Top Talents (2020R52001), and China Postdoctoral Science Foundation (BX2021272).

References

1. H. Köhler, "On Abbe's theory of image formation in the microscope," *Opt. Acta* **28**, 1691–1701 (1981).
2. H. Shroff, C. G. Galbraith, J. A. Galbraith, E. Betzig, "Live-cell photoactivated localization microscopy of nanoscale adhesion dynamics," *Nat. Meth.* **5**, 417–423 (2008).
3. S. A. Jones, S.-H. Shim, J. He, X. Zhuang, "Fast, three-dimensional super-resolution imaging of live cells," *Nat. Meth.* **8**, 499–508 (2011).
4. G. Vicidomini, P. Bianchini, A. Diaspro, "STED super-resolved microscopy," *Nat. Meth.* **15**, 173–182 (2018).
5. Y. Wu, H. Shroff, "Faster, sharper, and deeper: Structured illumination microscopy for biological imaging," *Nat. Meth.* **15**, 1011–1019 (2018).
6. C. Kuang, S. Li, W. Liu, X. Hao, Z. Gu, Y. Wang, J. Ge, H. Li, X. Liu, "Breaking the diffraction barrier using fluorescence emission difference microscopy," *Sci. Rep.* **3**, 1441 (2013).
7. G. Zhao, C. Kuang, Z. Ding, X. Liu, "Resolution enhancement of saturated fluorescence emission difference microscopy," *Opt. Exp.* **24**, 23596–23609 (2016).
8. M. Yoshida, Y. Kozawa, S. Sato, "Subtraction imaging by the combination of higher-order vector beams for enhanced spatial resolution," *Opt. Lett.* **44**, 883–886 (2019).
9. S. Sun, M. He, Z. Zhang, W. Wang, X. Yang, C. Kuang, X. Liu, "Enhancing the axial resolution of two-photon imaging," *Appl. Opt.* **58**, 4892 (2019).
10. S. Li, C. Kuang, X. Hao, Y. Wang, J. Ge, X. Liu, "Enhancing the performance of fluorescence emission difference microscopy using beam modulation," *J. Opt.* **15**, 5708 (2013).
11. Y. Cai, W. Liu, W. Yang, J. Xu, H. Yang, K. Shi, "Differential fluorescence microscopy by using a dynamic cylindrical-vector field," *Opt. Lett.* **46**, 2332–2335 (2021).
12. M. O. Lenz, H. G. Sinclair, A. Savell, J. H. Clegg, A. C. N. Brown, D. M. Davis, C. Dunsby, M. A. A. Neil, P. M. W. French, "3-D stimulated emission depletion microscopy with programmable aberration correction," *J. Biophoton.* **7**, 29–36 (2014).

13. Z. Zhang, S. Liu, M. He, Y. Huang, C. Kuang, Y. Han, X. Hao, X. Liu, "Three-dimension resolution enhanced microscopy based on parallel detection," *Appl. Sci.* **11**, 2837 (2021).
14. M. Mandal, R. Maji, S. Mukhopadhyay, "Increase of side band powers in parallel phase modulation by lithium niobate-based electro-optic crystal," *Braz J. Phys.* **51**, 738–745 (2021).
15. S. Sen, S. Mukhopadhyay, "A method of using a sharp cut and pointy electro-optic material for massive reduction of V_π voltage," *Optik* **126**, 5256–5259 (2015).
16. C. Li, "Electro-optic switcher based on dual transverse pockels effect and lithium niobate crystal," *IEEE Photon. Technol. Lett.* **29**, 2159–2162 (2017).
17. J. Cervantes-L, D. I. Serrano-Garcia, Y. Otani, B. Cense, "Mueller-matrix modeling and characterization of a dual-crystal electro-optic modulator," *Opt. Exp.* **24**, 24213–24224 (2016).
18. A. Liu, R. Jones, L. Liao, D. Samara-Rubio, D. Rubin, O. Cohen, R. Nicolaescu, M. Paniccia, "A high-speed silicon optical modulator based on a metal-oxide-semiconductor capacitor," *Nature* **427**, 615–618 (2004).
19. L. Liao, D. Samara-Rubio, M. Morse, A. Liu, D. Hodge, D. Rubin, U. D. Keil, T. Franck, "High speed silicon Mach-Zehnder modulator," *Opt. Exp.* **13**, 3129–3135 (2005).
20. L. Gu, W. Jiang, X. Chen, L. Wang, R. T. Chen, "High speed silicon photonic crystal waveguide modulator for low voltage operation," *Appl. Phys. Lett.* **90**, 071105 (2007).
21. N. Wang, T. Kobayashi, "Numerical study of the subtraction threshold for fluorescence difference microscopy," *Opt. Exp.* **22**, 28819–28830 (2014).
22. H. Dehez, M. Piche, Y. D. Koninck, "Resolution and contrast enhancement in laser scanning microscopy using dark beam imaging," *Opt. Exp.* **21**, 15912–15925 (2013).
23. S. Segawa, Y. Kozawa, S. Sato, "Resolution enhancement of confocal microscopy by subtraction method with vector beams," *Opt. Lett.* **39**, 3118–3121 (2014).
24. F. Gorlitz, S. Guldbrand, T. H. Runcorn, R. T. Murray, A. L. Jaso-Tamame, H. G. Sinclair, E. Martinez-Perez, J. R. Taylor, M. A. A. Neil, C. Dunsby, P. M. W. French, "easySLM-STED: Stimulated emission depletion microscopy with aberration correction, extended field of view and multiple beam scanning," *J. Biophoton.* **11**, e201800087 (2018).
25. A. Descloux, K. S. Gruβmayer, A. Radenovic, "Parameter-free image resolution estimation based on decorrelation analysis," *Nat. Meth.* **16**, 918–924 (2019).
26. D. C. Chan, "Mitochondria: Dynamic organelles in disease, aging, and development," *Cell* **125**, 1241–1252 (2006).